ISSN (Print) 1226-1750
ISSN (Online) 2233-6656
Journal of Magnetics 31(1), 70-78 (2026) https://doi.org/10.4283/JMAG.2026.31.1.70

Development and Characteristics of Portable Spatial Pulse Wave Velocity Monitoring Device Composed of MPG and PPG

Il-Ho Son[1,2,3], Jong-Gu Choi[3,4], and Sang-Suk Lee[1,3,4]*

[1]*Department of Oriental-Western Biomedical Engineering, Sangji University, Wonju 26339, Republic of Korea*
[2]*ForU Co., 45 Ipchun-ro, Wonju 26460, Republic of Korea*
[3]*Department of Digital Healthcare, Sangji University, Wonju 26339, Republic of Korea*
[4]*Department of Software, Sangji University, Wonju 26339, Republic of Korea*

(Received 2 January 2026, Received in final form 23 February 2026, Accepted 23 February 2026)

To monitor peripheral vascular conditions, we developed a portable measurement device that utilizes a magnetoplethysmogram (MPG) sensor implemented using a permanent magnet and a Hall element together with a photoplethysmogram (PPG) sensor to acquire peripheral pulse waveforms. The user's hand length (L_H) divided by the temporal delay ($\Delta\tau$) between two peaks of pulse signals obtained from the two sensors is used to calculate the spatial pulse wave velocity (SPWV). Analysis of the MPG and PPG output waveforms demonstrated stable, clearly periodic signals. We confirmed a meaningful property of SPWV from the preliminary pilot study measured by using the SPWV1 and SPWV2 monitoring devices. The difference between SPWV1 and SPWV2 arises from the pulse period correction. Because $\Delta\tau_{ave2} = \Delta\tau_{ave1} + T_{period}$, the denominator in the SPWV2 calculation increases, resulting in characteristically smaller SPWV2 values. For participant #1, SPWV1 remained within a relatively narrow band of 2.8 m/s~2.9 m/s, and SPWV2 within 27 cm/s~28 cm/s over the 60 min measurement window, demonstrating stable behavior. For participant #2, SPWV1 showed greater variability, increasing to a maximum at approximately 40 min before decreasing, while SPWV2 remained within 24 cm/s ~26 cm/s. The SPWV measurement system based on MPG-PPG is expected to enable convenient, non-invasive monitoring of peripheral vascular health.

Keywords: magnetoplethysmogram (MPG), permanent magnet, Hall element, photoplethysmogram (PPG), spatial pulse wave velocity (SPWV), peripheral vasculature

1. Introduction

Pulse wave velocity (PWV), defined as the speed at which the pressure wave generated by cardiac ejection propagates along the arterial wall, is widely recognized as a key indicator of arterial stiffness [1-3]. Increased arterial stiffness is closely associated with the onset and prognosis of cardiovascular disorders, including hypertension, diabetes, and dyslipidemia [1, 3, 4]. Conventional PWV assessments, such as carotid–femoral PWV (cf-PWV), have traditionally focused on evaluating aortic stiffness [1, 3]. However, peripheral vascular status provides important insight into microcirculatory function and local tissue health, and plays a critical role in conditions such as diabetic microangiopathy [2, 5]. Existing aortic PWV measurement systems are typically bulky and complex, limiting their suitability for continuous monitoring during daily activities [3, 4]. Consequently, there is a growing demand for portable, user-friendly devices capable of non-invasive, real-time monitoring of peripheral vascular function [6, 7].

This study addresses this need by developing a magnetoplethysmogram (MPG)-photoplethysmogram (PPG) based portable device capable of measuring spatial pulse wave velocity (SPWV), a metric that reflects peripheral vascular characteristics [8-11]. The MPG sensor detects magnetic field variations induced by pulsatile changes in vascular pressure, while the PPG sensor measures optical absorption changes associated with blood volume fluctuations. By computing the temporal delay ($\Delta\tau$) between the first peak and the second peak for the continuous pulse waveforms of MPG and PPG signals, respectively, the system enables precise estimation of spatial pulse transit time within the peripheral

*Corresponding author: Tel: +82-33-730-0415
Fax: +82-33-738-7610, e-mail: sslee@sangji.ac.kr (S. S. Lee)

vasculature. Ultimately, we validate the measurement accuracy and continuous monitoring capability of the wrist-worn portable SPWV device, demonstrating its potential utility for clinical and everyday assessment of peripheral vascular health.

2. Experimental Methods

A Hall element clip-type pulsimeter called MPG is a device that quantitatively measures the pulse waveform by covering the clips on the radial artery where the pulse is beating and detecting the magnetic field change caused by the minute movement of the artery with a permanent magnet (PM) and a Hall element [6-11]. It is a digitalization of the traditional hand-held pulse wave method, which is used for oriental medicine diagnosis by showing the strength and speed of the pulse in waveforms. It detects pulses by attaching a clip sensor to the radial artery. Applying the magnetic field principle, the permanent magnet within the clip-type pulsimeter changes its position according to the minute movement (pressure change) of the pulse, causing the ambient magnetic field to change [8, 10, 12]. The Hall element generates a pulse waveform by converting this magnetic field change into an electrical signal by the Hall element. Quantitative measurements can provide consistent pressure (spring pressure of the tongs) rather than holding it by hand, thereby obtaining highly reproducible and objective pulse information [6, 7, 11]. The field of application is oriental medicine diagnosis, which is diagnosed by analyzing various pulse conditions (fractures) such as pulse in waves. It is used for the western-eastern convergence medical research with electrocardiogram (ECG), MPG, and PPG, and is used for various studies such as developing a two-hand pulse system and extracting respiratory rate by developing a system [6, 7, 13, 14].

Figs. 1(a), 1(b), 1(c), and 1(d) show the side view of the permanent magnet and the silicone rubber housing, (b) the front view of surface, (c) the inner view of surface, and the permanent magnet and silicone rubber housing placed on the radial artery near the wrist, respectively. Figs. 1(e), 1(f), 1(g), 1(h), and 1(i) show the permanent magnet housing placed near on the radial artery, (f) the detailed view of the permanent magnet housing placed on the radial artery near the wrist, (g) a schematic of the systematic of operating principal pulse meter's pulse-sensing mechanism Hall element and permanent magnet

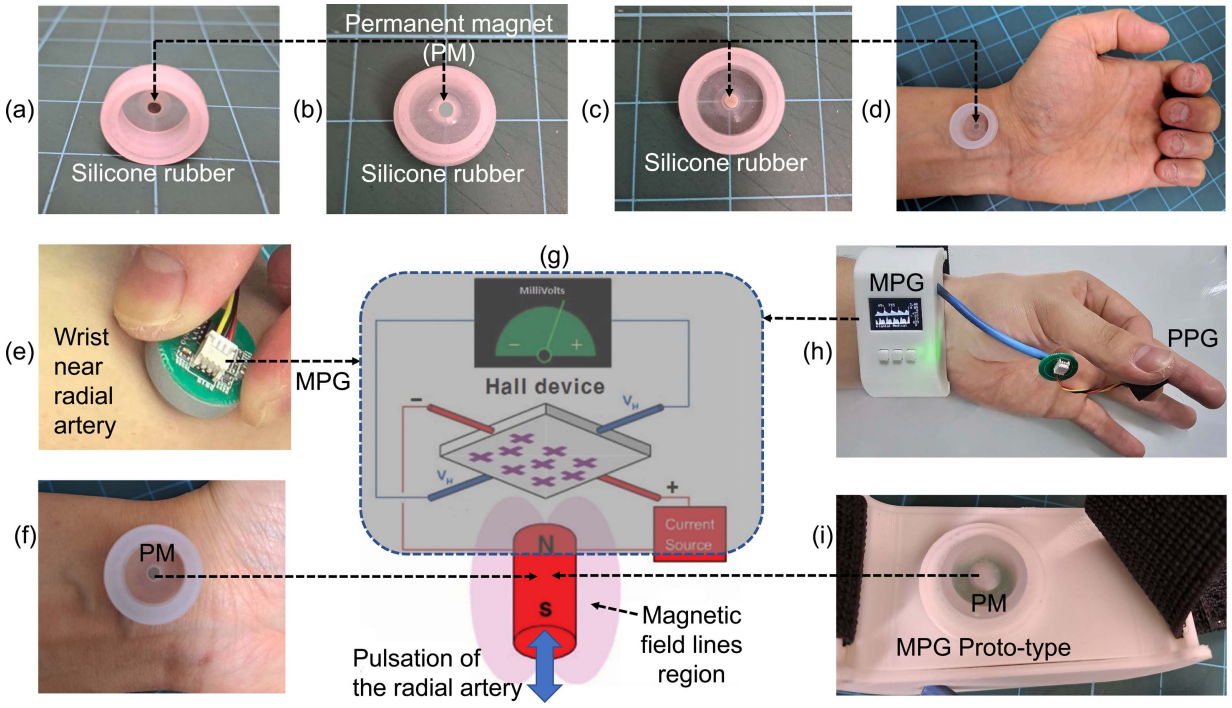

Fig. 1. (Color online) (a) The side view, (b) front view, (c) inner view, (d) top view of one permanent magnet and silicone rubber housing placed on the radial artery near the wrist, (e) contacting feature the permanent magnet housing of the MPG measuring part near the radial artery, (f) detailed view of the permanent magnet housing placed on the radial artery near the wrist, (g) a schematic the pulse-sensing mechanism using Hall element and permanent magnet [15], (h) the measuring feature by using the MPG prototype, and (i) the detailed view of the permanent magnet and silicone rubber.

[15], (h) the measurement of the MPG prototype, and (i) the detailed view of the permanent magnet and silicone rubber of the MPG prototype, respectively.

3. Results and Discussion

Fig. 2 illustrates the major components required for operating the MPG and PPG sensors, as well as the process of acquiring pulse waveforms. The sensor configuration was designed such that the MPG sensor is positioned on the wrist to capture mechanical arterial pulsations, while the PPG sensor is placed on the finger to measure blood volume changes. Fig. 2(a) shows the Hall element used in this study, which is the A1391 model manufactured by Allegro Microsystems, a micro-power 3 V linear Hall-effect sensor IC [8, 12, 16, 17]. The displacement of the permanent magnet attached to the radial artery site can differ according to the pulsation strength of the radial artery. To accommodate this intersubject variability, we selected an A1391 sensor representing the lowest sensitivity (1.25 mV/G) of the A139x series to ensure stable signal collection without saturation. To detect the minute voltage variations induced by small skin-surface displacements resulting from radial artery pulsation, the sensor output was amplified by a factor of 100 using an operational amplifier. An analog filtering circuit was subsequently applied to isolate the principal frequency components of the pulse wave signal, which lie in the range of 0.5-10 Hz [6-8]. Specifically, a high-pass filter (HPF) with a cutoff frequency of 0.5 Hz was employed to suppress baseline wander. In comparison, a low-pass filter (LPF) with a cutoff frequency of 15 Hz was used to attenuate high-frequency noise components unrelated to the pulse waveform. To minimize signal distortion and ensure accurate digitization, the amplified and filtered signal was sampled at a rate of 100 samples per second (Sps).

Meanwhile, Fig. 2(b) shows the switch used for controlling the measurement device and the USB-C module employed for bidirectional data and control message communication between the device and a PC, as well as for battery charging. These two electronic components were selected with consideration of compactness, ease of miniaturization, and component availability. Accordingly, a widely used 5.2 mm micro tact switch and a modularized USB-C connector were adopted. In particular, although USB-C connectors are generally more challenging to implement than other types of USB connectors, the use of a pre-assembled module facilitated convenient integration into the system. To supply operating power to the

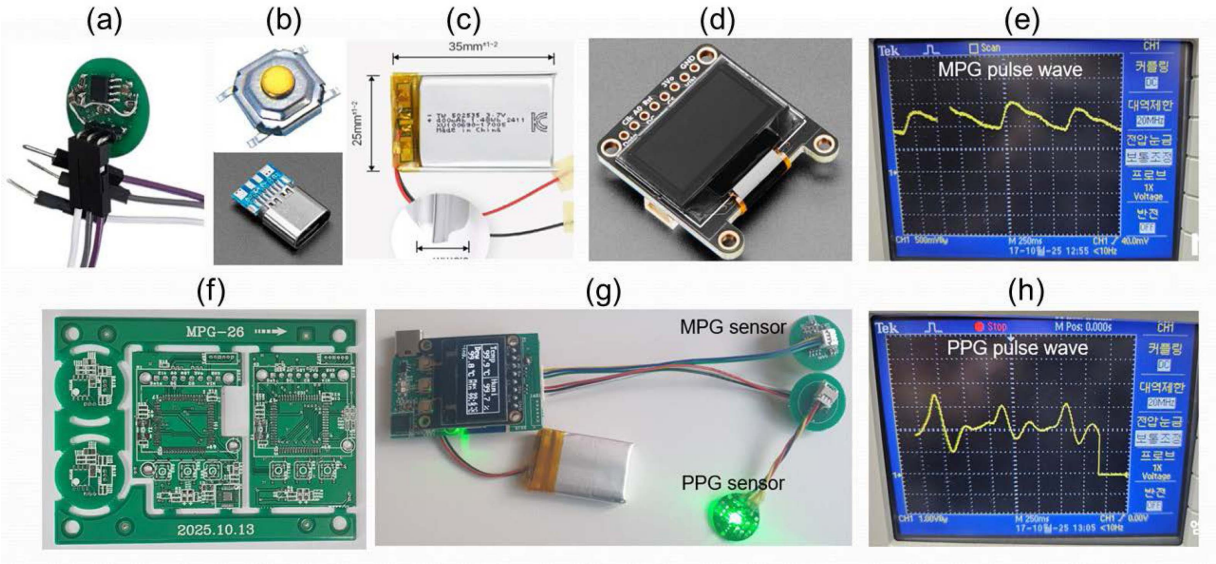

Fig. 2. (Color online) Components required to drive MPG and PPG sensors and the pulse waveform acquisition process. (a) A1391 model Hall element and analog filter circuit, (b) USB-C module for control switch and data transmission/reception and battery charging power connection, (c) lithium polymer battery, (d) OLED graphic display, (e) MPG pulse waveform displayed on an oscilloscope as an output signal from a magnetic field sensor module, (f) PCB board consisting of a main board for driving MPG and PPG, sensor data collection power management, operation control signal input, measurement signal graph and data information display on a display screen, and data communication with a PC, (g) assembly photo of the entire hardware configuration of the MPG-PPG sensors, and (h) PPG pulse waveform displayed on an oscilloscope as an Amp output signal of the Amp module for the PPG sensor.

portable MPG prototype, a lithium-polymer battery with a nominal voltage of 3.7 V, a capacity of 400 mAh, and dimensions of 35 mm × 25 mm was employed, as illustrated in Fig. 2(c). This battery was chosen to balance device portability, compact form factor, and sufficient operating time. Fig. 2(d) presents the display module used to allow users to monitor the real-time measurement signal status and numerical measurement values during device operation. A monochrome 0.96-inch 128 × 64 OLED graphic display (STEMMA QT, Adafruit Industries) was utilized. Among various graphic display options, this module offers low power consumption and a small physical footprint, which are advantageous for device miniaturization. Furthermore, its 128 × 64 resolution enables simultaneous visualization of both MPG and PPG waveform graphs, numerical measurement data, and alphanumeric information, making it well-suited for the proposed system.

Fig. 2(e) presents an oscilloscope measurement captured to verify the output signal of the magnetic field sensor module shown in Fig. 2(a). Examination of the measured waveform confirms that it clearly exhibits the characteristic feature points required for pulse wave analysis, including the onset point, systolic peak, reflected wave point, and dicrotic notch. In addition, the signal amplitude exceeded 500 mV, and the entire waveform remained within the designed measurement range of 5 V, thereby validating that the fabricated sensor module is suitable for practical use. Fig. 2(f) shows a photograph of the printed circuit board (PCB) designed and fabricated based on the comprehensive requirements established through unit testing. The system consists of a MPG module, which conditions the magnetic field sensor output into a signal suitable for accurate measurement and is dimensioned for ease of mechanical attachment; an amplifier (Amp) module, which compensates for the relatively noisy and coarse output characteristics of the previously used PPG module; and a main board responsible for sensor data acquisition, power management, operational control signal input, graphical and numerical display of measured signals on the screen, and data communication with a PC.

Fig. 2(g) presents an assembled photograph of the complete hardware configuration for MPG–PPG operation. The system consists of a main board incorporating the main control unit (MCU), display module, switch control interface, USB communication interface, power management unit, and battery charging circuitry. The MPG module, positioned at the wrist on the palmar side and connected to the main board located on the dorsal side of the hand, and the PPG module, positioned at the fingertip, are each interfaced via two 4-pin cables. The configuration also includes a battery to supply power to the portable device, thereby completing the integrated wearable system. To verify the suitability of the amplifier (Amp) module designed to condition the previously used PPG module's relatively noisy output into a signal appropriate for analysis, the amplified PPG output was measured using an oscilloscope, as shown in Fig. 2(h). Inspection of the measured waveform demonstrates that it clearly represents the characteristic feature points required for pulse wave analysis, including the onset point, peak point, reflected wave point, and dicrotic notch. Moreover, the signal amplitude exceeded 2 V, and the entire waveform remained within the designed measurement range of 5 V, thereby confirming that the fabricated sensor and amplifier module are suitable for practical application.

For experimental validation and data acquisition, the developed device was used to perform SPWV measurements. Participants wore the smart measurement unit on the wrist, while the PPG sensor was positioned on the finger. To evaluate continuous measurement performance, SPWV1 and SPWV2 were repeatedly recorded at fixed intervals over a 60-min period, and their temporal variations were analyzed. Fig. 3 presents the external and internal structure of the smart SPWV measurement device prototype, along with its wearability. Fig. 3(a) shows the front housing and strap fabricated using a 3D printer. Fig. 3(b) depicts the internal connector components. Figs. 3(c), 3(d), and 3(e) illustrate the rear housing and strap, the acquisition of radial artery pulse waveforms using the MPG sensor, and the device worn on the wrist during actual measurement, respectively.

Regarding pulse waveform characteristics, both the MPG and PPG signals exhibited stable and well-defined pulsation formation. The MPG signal exhibited distinct peaks and a regular periodic structure, enabling the clear identification of the onset of pulse wave propagation. This stability was further confirmed through oscilloscope traces (Fig. 2(e)). The PPG signal similarly displayed pronounced peaks with a consistent temporal delay relative to the MPG waveform, as verified by the oscilloscope data (Fig. 2(h)). These well-resolved signal features enable precise estimation of $\Delta\tau$, which is essential for accurate PWV computation [2-4]. The portable measurement device was designed with an emphasis on everyday usability, aiming to provide a level of comfort and wearability comparable to mainstream consumer devices such as the Galaxy Watch or Apple Watch [4, 13, 14]. This consideration ensures that users can perform continuous peripheral vascular monitoring with minimal inconvenience during daily activities.

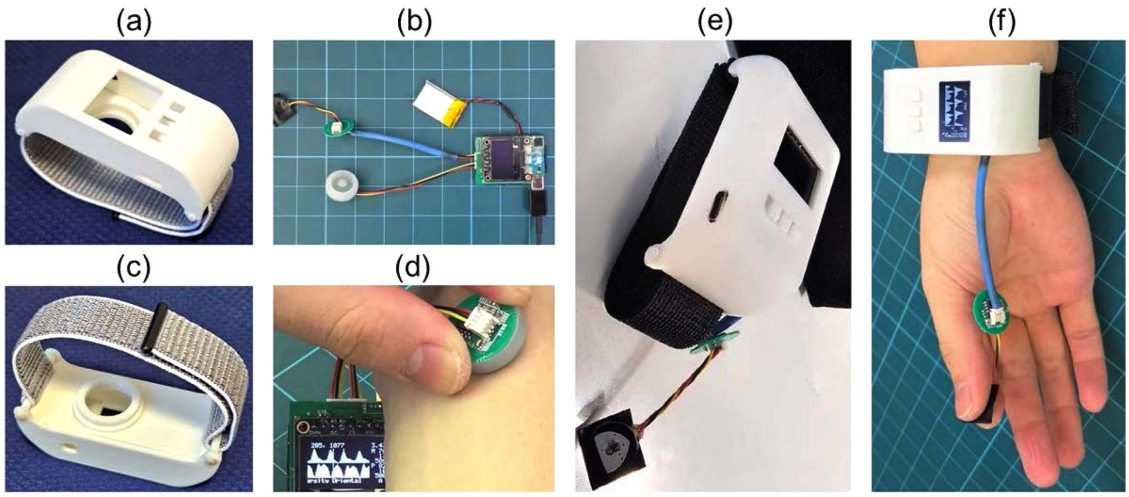

Fig. 3. (Color online) The exterior and internal components of the portable SPWV meter prototype, as well as its wearable appearance. (a) Front prototype exterior and straps fabricated using a 3D printer, (b) Built-in connecting components, (c) Rear prototype exterior and straps fabricated using a 3D printer, (d) Pulse waveforms of the radial artery and of the finger capillaries obtained using MPG and PPG sensors, respectively, (e) Actual measurements by using the prototype of portable SPWV monitoring device.

In this study, we developed a smart SPWV measurement device incorporating both MPG and PPG sensors. The system is built around a microcontroller platform and integrates on-board signal processing and PWV computation capabilities. The hardware consists of a sensor module, a main circuit board (MPG-26 PCB), a battery-powered supply, and a user interface comprising an OLED display and control buttons. Fig. 4 illustrates the operating principle and algorithm of the MPG–PPG based on the SPWV device. Fig. 4(a) shows the device worn on

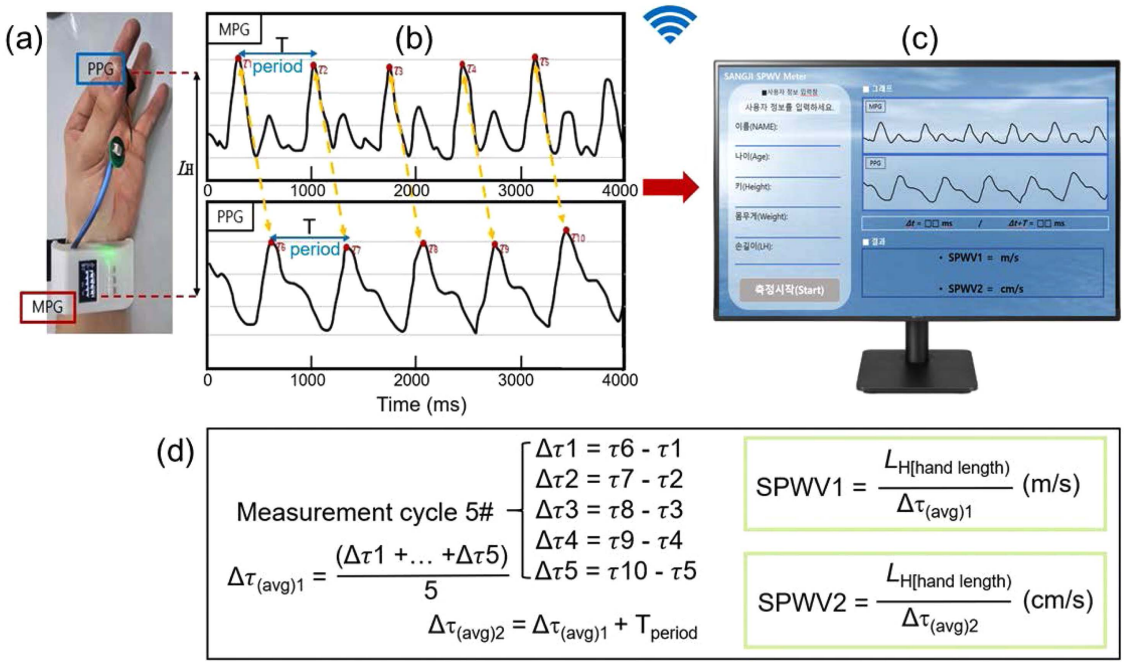

Fig. 4. (Color online) The operating principle and algorithm of the MPG-PPG based on the portable SPWV monitoring device (a) Appearance of the measuring device when worn, (b) Appearance of continuous form of MPG and PPG pulse waves and time difference between peaks, (c) Display screen showing input and output values and pulse wave form transmitted to PC wirelessly via Wi-Fi, (d) Definition of SPWV1 and SPWV2 and calculation algorithm formula.

the wrist; Fig. 4(b) presents representative MPG and PPG pulse waveforms and their corresponding peak-to-peak temporal delays. Fig. 4(c) displays the waveform visualization and input/output parameters transmitted wirelessly to a PC via Wireless Fidelity (Wi-Fi). Fig. 4(d) outlines the definitions of SPWV1 and SPWV2 along with their respective computational formulas. Pulse wave acquisition is performed simultaneously using both sensors. The MPG waveform exhibited stable morphology with clearly identifiable peaks ($\tau1$, $\tau2$, $\tau3$, $\tau4$, $\tau5$). Similarly, the PPG waveform demonstrated stable periodicity with distinct peaks ($\tau6$, $\tau7$, $\tau8$, $\tau9$, $\tau10$), closely matching the temporal pattern observed in the MPG signal as shown in Fig. 4.

Although the initial prototype adopted a wrap-around wrist configuration, this design was found to be sub-optimal in terms of comfort. To improve user experience, we redesigned the device with a more ergonomic form factor tailored for comfortable and stable continuous wear. Sensor placement and external housing were refined through iterative 2D and 3D design processes, followed by dimensional optimization to accommodate the internal circuitry. A complete 3D model of the enclosure was produced, and a prototype casing was fabricated. After printing the exterior housing, the circuit board dimensions were fitted and validated. The strap was also redesigned to address limitations of the previous version, which was narrow, rigid, and difficult to adjust. The new elastic black strap allows flexible expansion and contraction, enabling secure and comfortable wear across a wide range of wrist sizes. After assembly, the MPG and PPG waveform acquisition was verified to confirm proper device functionality.

The fabricated device uses the ATmega128A Microcontroller Unit to collect data by sampling two signals output from two sensor modules, MPG and PPG, 100 times per second, and smoothing them using a moving average filter with a width of 5 to maintain the continuity of the signal. The acquired data is displayed in real-time graphs and heart rate on the OLED module, which is a display device. To display the real-time graph, a scaled value was calculated by establishing a proportional equation to fit the graph display area range of the display device. Due to the graph size varying depending on the person measuring or the intensity of wearing the device, the graph may go beyond the screen and the overall graph shape may not be visible, or may be displayed too small on the screen to make it inconvenient to check the signal. To prevent this, the maximum and minimum values of the measured values are stored for 5 s and automatically scaled every 5 s according to the maximum and minimum values to always display them in a full screen.

In order to calculate the difference in peak point arrival time between the two sensor signals, the start and end of each signal cycle must be known. The time of the maximum signal between the start and the end must be extracted and compared. To do so, there must be a reference point to be judged as the start of one cycle. The algorithm identifies the reference point as the time value where the data reaches its maximum during four samples of signal increase within the interval between the previous and current start points, and the time difference between the MPG and PPG peak points is calculated and stored. From the time when the stored time value exceeds 10, the average of eight values excluding the maximum and minimum two values among the recent 10 data is displayed using the time difference between the MPG and PPG peak points as the result of the time difference. Using the start points obtained in this calculation, the heart rate can be obtained through the time between the previous start points, and the two heart rates obtained through each signal of MPG and PPG can be compared to check whether the measurement is performed properly. In order to easily check whether the data of the maximum value were obtained properly, a certain value was added to the obtained maximum value. The maximum value was displayed on the OLED display to confirm that the maximum value was displayed pointedly, and the data of the maximum value were properly specified. When displaying on the OLED display, various information was displayed by dividing the OLED resolution of 128 × 64 into 5 zones. The first zone displays the results of analysis through the measured data, the second zone displays the real-time PPG signal graph, the third zone displays the real-time MPG graph, and the fourth zone displays real-time numerical data of PPG and MPG signals. The heart rate is calculated using two real-time numerical data of PPG and MPG signals, and the fifth zone displays other device manufacturing information.

Fig. 5 summarizes representative cases and the corresponding analytical results. Fig. 5(a) shows the display output of the wrist-worn SPWV measurement device. Fig. 5(b) presents real-time SPWV1 and SPWV2 values for participant #1. Figs. 5(c) and 5(e) illustrate the temporal variations of SPWV values for participants #1 and #2, respectively. Fig. 5(d) displays the real-time output for participant #2. For participant #1 (Fig. 5(c)), SPWV1 varied within approximately 2.85 ± 0.5 m/s, while SPWV2 ranged from 27.5 ± 0.5 cm/s. For participant #2 (Fig. 5(e)), SPWV1 fluctuated between roughly 10 ± 0.5 m/s, whereas SPWV2 ranged from 25 ± 1.0 cm/s.

To evaluate the continuous measurement performance of the developed portable SPWV monitoring device,

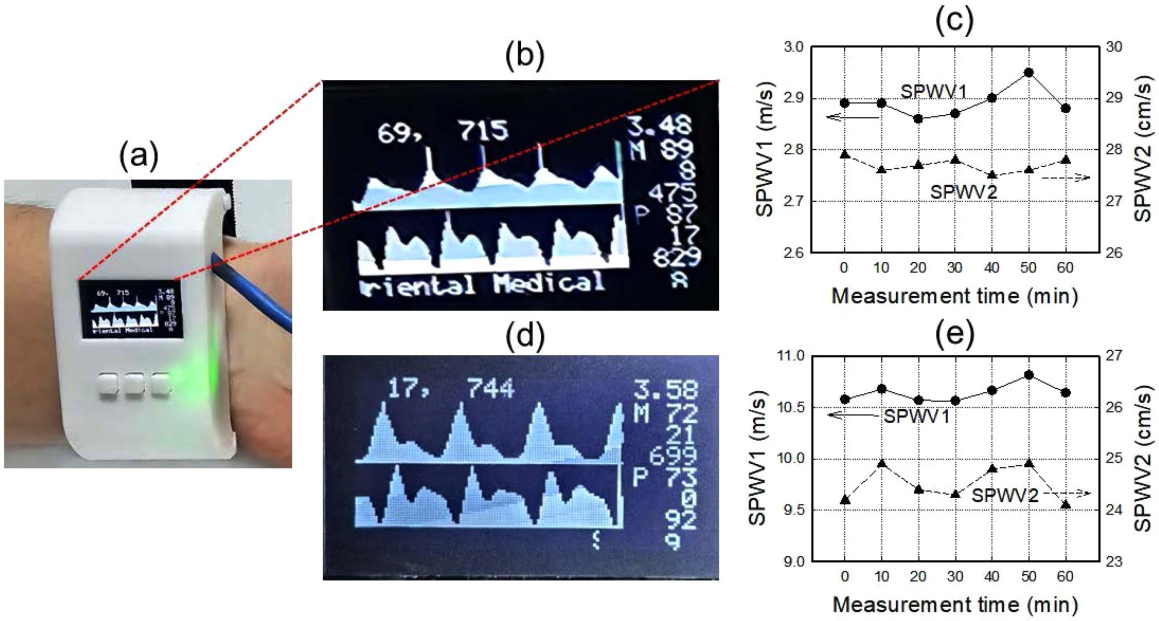

Fig. 5. (Color online) Analysis of measurement cases and results of two subjects from a previous study experiment. (a) a wrist-worn portable SPWV1 and SPWV2 measuring instrument, (b) the actual display of temporal delay times ($\Delta\tau_{ave1}$, $\Delta\tau_{ave2}$) and MPG and PPG waveforms for participant #1, (c) change in SPWV1 in the range of about 2.8 m/s to 2.9 m/s and change in the range of about 27 to 28 cm/s SPWV2 in participant #1, (d) the actual display of temporal delay times ($\Delta\tau_{ave1}$, $\Delta\tau_{ave2}$) and MPG and PPG waveforms for participant #2, (e) change in the range of about 9.5 to 10.5 m/s of SPWV1 and change in the range of about 24 to 26 cm/s of SPWV2 in participant #2.

SPWV1 and SPWV2 were repeatedly measured using the prototype, and the results are presented in Figs. 5(c) and 5(e). Two male participants in their 20s were enrolled in this preliminary pilot study, and their individual hand lengths (L_H), used for SPWV computation, are displayed alongside the corresponding graphs. For participant #1, minimal changes were observed overall, although a slight elevation in both SPWV1 and SPWV2 values was noted following ingestion. Participant #2 similarly exhibited measurable differences, indicating that the developed device is capable of detecting subject-specific variations in peripheral pulse dynamics.

SPWV values can be summarized as follows. For participant #1, SPWV1 remained within a relatively narrow band of 2.8 m/s~2.9 m/s, and SPWV2 within 27 cm/s~28 cm/s over the 60 min measurement window, demonstrating stable behavior. For participant #2, SPWV1 showed greater variability, increasing to a maximum at approximately 40 min before decreasing, while SPWV2 remained within 24 cm/s~26 cm/s. These observations highlight that SPWV1 tends to exhibit larger fluctuations than SPWV2, likely due to its direct dependence on $\Delta\tau$ without cycle-based correction [1, 5, 18].

SPWV1 is highly sensitive to even minor variations in $\Delta\tau$, leading to relatively large fluctuations in the output. In contrast, SPWV2, which incorporates the pulse period as a correction factor, consistently exhibited stable behavior within a narrower range. Therefore, SPWV2 is a more appropriate and preferred biomarker for continuous and long-term monitoring than SPWV1. While SPWV1 may be useful for capturing instantaneous changes, SPWV2 provides superior analytical stability and reproducibility by effectively attenuating measurement noise. Consequently, for the practical application of portable peripheral vascular monitoring devices, SPWV2 offers a more reliable and robust indicator for assessing a patient's hemodynamic status. The difference between SPWV1 and SPWV2 arises from the pulse period correction. Because $\Delta\tau_{ave2} = \Delta\tau_{ave1} + T_{period}$, the denominator in the SPWV2 calculation increases, resulting in characteristically smaller SPWV2 values. Overall, the continuous measurement data demonstrate that the developed device successfully tracks temporal variations in peripheral circulatory dynamics. Figs. 5(b) and 5(d) further confirm the real-time monitoring capability by showing the calculated SPWV values displayed alongside the acquired pulse waveforms.

The conventional SPWV1 calculates velocity using only the time delay between the MPG and PPG sensors as the denominator. However, peripheral pulse signals often

exhibit subtle fluctuations in $\Delta\tau$ values due to slight vibrations at the measurement site or ambient noise. Because $\Delta\tau$ is a relatively small value, even these small fluctuations can significantly distort the calculated velocity. To address this issue, we used SPWV2, which includes the pulse period (T_{period}) in the denominator. Experimental results showed that SPWV1 exhibited high sensitivity and large variability, while SPWV2 exhibited stable behavior within a narrow range throughout the measurement. This suggests that SPWV2 effectively attenuates transient noise and reflects consistent peripheral hemodynamic characteristics by leveraging the unique pulse periodicity of an individual. Therefore, SPWV2 provides a robust analytical foundation for objective and reproducible assessment in long-term continuous monitoring environments.

Using the custom-designed PCB developed by our research team, Wi-Fi and Bluetooth connectivity were successfully integrated, enabling seamless communication with a remote server and real-time data transmission to a PC. Building on this foundation, the established SPWV algorithm will be further refined and applied in upcoming clinical studies. Regarding the future development potential of the portable SPWV monitoring device, the priority is to solidify the conceptual framework of SPWV through diverse clinical experiments and validation studies. Accumulating empirical evidence will support the robustness and clinical relevance of the SPWV measurement. Subsequently, efforts will be directed toward further miniaturization of the device, optimizing efficiency, and reducing overall weight. Enhancements in battery performance will also be pursued to enable continuous wear for more than 24 hours, similar to commercial consumer devices such as the smartwatch, thereby facilitating long-term peripheral vascular monitoring in daily life.

Despite these promising prospects, we acknowledge that the small sample size (N=2) in this study serves as a limitation for broad clinical validation. As a proof of concept, this work primarily focuses on the technical feasibility and analytical stability of the SPWV2 metric. Future research will involve a larger and more diverse demographic to correlate SPWV2 with gold-standard measurements, such as carotid-femoral PWV (cf-PWV), to further establish its diagnostic accuracy and clinical utility.

5. Conclusions

To monitor peripheral vascular conditions, we developed a smart measurement device that utilizes a MPG sensor implemented using a permanent magnet and a Hall element, together with a PPG sensor to acquire peripheral pulse waveforms. The temporal delay ($\Delta\tau$) between the pulse signals obtained from the two sensors, combined with the user's L_H (hand length), is used to calculate the SPWV. Analysis of the MPG and PPG output waveforms demonstrated stable and clearly periodic signals. Using the newly developed wrist-worn the portable SPWV monitoring device, we continuously measured SPWV and confirmed the temporal trends of SPWV1 and SPWV2. The MPG-PPG based on the portable SPWV measurement system developed in this study is expected to enable convenient, non-invasive monitoring of peripheral vascular health. Continuous measurements performed with the wrist-worn prototype demonstrated that the device successfully tracked temporal variations in both SPWV1 and SPWV2. These findings indicate that the MPG–PPG based on the SPWV device enables convenient, real-time assessment of peripheral vascular dynamics.

Acknowledgements

This research is the result of an integrated project supported by the Entrepreneurship Club Business and Capstone Design Class of the Department of Digital Healthcare at Sangji University in 2025.

References

[1] R. Asmar, A. Benetos, G. M. London, C. Hughe, Y. Weiss, J. Topouchian, B. Laloux, and M. Safar, Blood Press. **4**, 48 (1995).
[2] Q. Yu, J. Zhou, and Y. C. Fung, Am. J. Physiol. Heart Circ. Physiol. **265**, 52 (1993).
[3] A. Yamashina, H. Tomiyama, T. Arai, Y. Koji, M. Yambe, H. Motobe, Z. Glunizia, Y. Yamamoto, and S. Hori, Hypertens. Res. **26**, 801 (2003).
[4] Y. R. Kim, K. J. Cheon, J. S. Kim, H. S. Moon et al., Int. J. Arrhythm. **19**, 145 (2018).
[5] R. Fernández-Verdejo, G. Sanchez-Delgado, and E. Ravussin, Annu. Rev. Nutr. **44**, 51 (2024).
[6] S. S. Lee, D. H. Nam, Y. S. Hong, W. B. Lee, I. H. Son, K. H. Kim, and J. G. Choi, Sensors **11**, 1784 (2011).
[7] D. H. Nam, W. B. Lee, Y. S. Hong, and S. S. Lee, Sensors **13**, 4714 (2013).
[8] I. H. Son and S. S. Lee, J. Kor. Magn. Soc. **21**, 104 (2011).
[9] M. C. Ahn, J. G. Choi, I. H. Son, S. S. Lee, and K. H. Kim, J. Kor. Magn. Soc. **20**, 106 (2010).
[10] S. S. Lee, M. C. Ahn, and S. H. Ahn, J. Magn. **14**, 132 (2009).
[11] S. S. Lee, I. H. Son, J. G. Choi, D. H. Nam, Y. S. Hong, and W. B. Lee, J. Kor. Phys. Soc. **58**, 349 (2011).

[12] I. H. Son, G. I. Kim, Y. C. Kim, H. Lee, and S. S. Lee, J. Kor. Magn. Soc. **35**, 40 (2025).
[13] S. S. Lee, R. G. Choi, W. T. Kim, M. W. Shin, J. G. Choi, M. Hasan, and B. Jung, AIP Adv. **14**, 025009 (2024).
[14] G. I. Kim, Y. C. Kim, H. J. Lee, Y. H. Kim, S. H. Baek, J. G. Choi, D. Y. Park, B. Jung, and S. S. Lee, J. Magn. **29**, 441 (2024).
[15] D. J. Lee, S. H. Kim, J. H. Jeong, and S. S. Lee, J. Kor. Magn. Soc. **28**, 105 (2018).
[16] R. G. Choi, W. T. Kim, S. S. Lee, D. Sunwoo, and B. Jung, J. Kor. Magn. Soc. **33**, 69 (2023).
[17] K. H. Kim and S. S. Lee, J. Magn. **20**, 47 (2015).
[18] G. I. Kim, J. G. Choi, B. Jung, and S. S. Lee, New Phys.: Sae Mulli, **74**, 1210 (2024).